Effective Temperature Determination

Barry Smalley

Abstract Effective temperature is the most important stellar atmospheric parameter. It is an essential prerequisite for detailed spectroscopic analyses. A discussion of the methods for determining effective temperature using stellar spectra is presented. The use of Balmer line profiles is explored and the role of spectral line depth ratios outlined. Equivalent width measurements are a powerful tool for determining effective temperature, via the excitation potential method. This is explored in detail including the sensitivity to surface gravity and metal abundance. The discussion leads to the use of spectrum synthesis fitting to determine effective temperature.

Keywords Line: profiles · Stars: atmospheres · Stars: fundamental parameters · Techniques: spectroscopic

1 Effective Temperature

The effective temperature ($T_{\rm eff}$) of a star is physically related to the total radiant power per unit area at stellar surface ($F_\star$):

$$\sigma {T_{\rm eff}}^4 = \int_0^\infty F_\lambda d\lambda = F_\star = \frac{L}{4\pi R^2}.$$

It is the temperature of an equivalent black body that gives the same total power per unit area, and is directly given by stellar luminosity (L) and radius (R).

Since there is not true 'surface' to a star, the stellar radius can vary with the wavelength of observation and nature of the star. Radius is taken as the depth of

B. Smalley (✉)
Astrophysics Group, Keele University, Keele, Staffordshire ST5 5BG, UK
e-mail: b.smalley@keele.ac.uk

E. Niemczura et al. (eds.), *Determination of Atmospheric Parameters of B-, A-, F- and G-Type Stars*, GeoPlanet: Earth and Planetary Sciences,
DOI: 10.1007/978-3-319-06956-2_8,

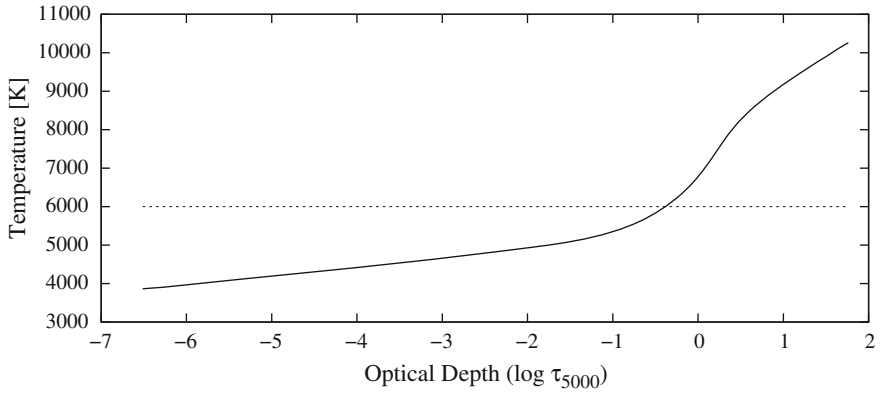

Fig. 1 The depth dependence of atmospheric temperature with monochromatic optical depth at 5,000 Å. Based on model atmosphere with $T_{\rm eff}$ = 6,000 K. The horizontal dashed line indicates a temperature of 6,000 K which intercepts the model at optical depth around $\log \tau_{5000} = -0.5$, corresponding the depth of formation of the continuum flux

formation of the continuum, which in the visible region is approximately constant for most stars (Gray 2008).

The effective temperature is broadly that of the atmospheric layer in which the continuum is formed. The temperature of line-forming region is lower than $T_{\rm eff}$ (Fig. 1). In addition, spectral lines are formed at differing depths and temperatures, making them useful as $T_{\rm eff}$ diagnostics.

2 The Paschen Continuum

The most direct method of determining stellar $T_{\rm eff}$ is by using absolute flux measurements. This requires moderate-resolution flux-calibrated spectra or spectrophotometry. However, even if only relative fluxes are available, they can be used to determine $T_{\rm eff}$, since the Paschen continuum is sensitive to temperature variations (Fig. 2). This is also the basis for $T_{\rm eff}$-colour calibrations. This is covered in more detail in Chap. 10

3 Temperatures from Balmer Line Profiles

The Balmer lines provide an excellent $T_{\rm eff}$ diagnostic for stars cooler than about 8,000 K due to their virtually null gravity dependence (Gray 2008; Heiter et al. 2002). By fitting theoretical profiles to observations, we can determine $T_{\rm eff}$. For stars hotter than 8,000 K, however, the profiles are sensitive to both temperature and gravity. For

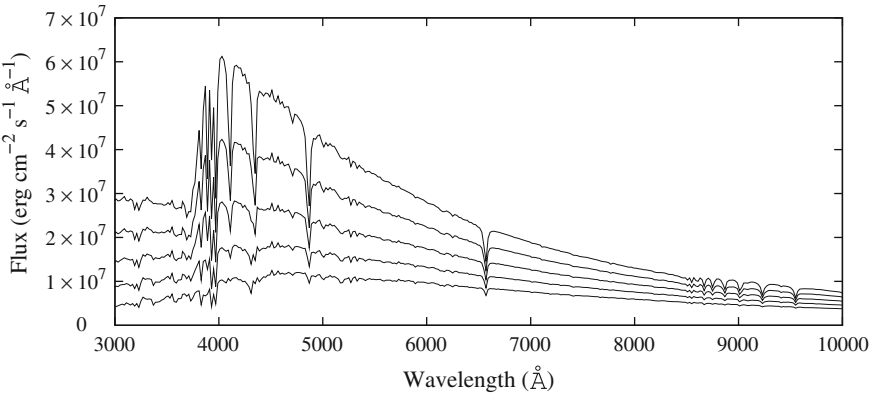

Fig. 2 The variation of stellar flux with $T_{\rm eff}$, ranging from 6,000 K (*bottom*) to 8,000 K (*top*) in steps of 500 K

these stars, the Balmer lines could be used to obtain values of surface gravity ($\log g$), provided that their $T_{\rm eff}$ can be determined from a different method.

The broad Balmer lines require careful continuum determination, because the true profile shape must be preserved (Smith and van't Veer 1988). Echelle spectra usually give poor profiles due to curved orders and the merging process in pipeline reductions (Bruntt et al. 2010). Hence, single-order medium-resolution spectra are preferred.

3.1 Examples of Balmer Line Fitting

Figure 3 shows a fit to the Solar Hα profile. Note that the core region (approximately ± 1 Å) is not used in the fitting, since it is formed high in the stellar atmosphere and subject to NLTE effects. On first inspection, the known $T_{\rm eff}$ for the Sun produces an acceptable fit. This would be especially true at higher noise levels. However, on closer inspection, the best fit is with a $T_{\rm eff}$ that is ~ 60 K lower than actual Solar value. Model deficiencies, for example the treatment of line-broadening or convection theory, can lead to temperature values that disagree with the true or fundamental value (see for example Cayrel et al. 2011). Hence, as with all model-dependent methods, they should be tested against stars with known model-independent $T_{\rm eff}$ values.

KIC 11772920 (TYC 3565-1235-1) is a slowly rotating G-type star (Appourchaux et al. 2012). Figure 4 shows a HERMES (Raskin et al. 2011) spectrum with the fit to the Hα profile. With the exception of the core, the profile is well fitted with a $T_{\rm eff}$ of 5,300 K.

KIC 11090405 (BD+48 2925) is a rapidly rotating A-type star exhibiting δ Sct type pulsations (Uytterhoeven et al. 2011). Figure 5 shows that the Hα profile indicates

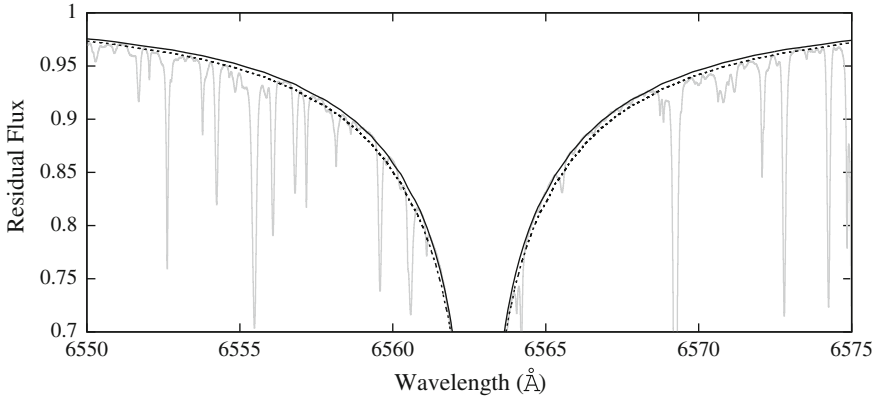

Fig. 3 The KPNO Solar Atlas Hα profile (*grey line*). The *dotted-line* is the fit using the parameters for the Sun ($T_{\rm eff}$ = 5,777 K and $\log g$ = 4.44), while the *black line* is the 'best-fitting' profile with $T_{\rm eff}$ = 5,720 K

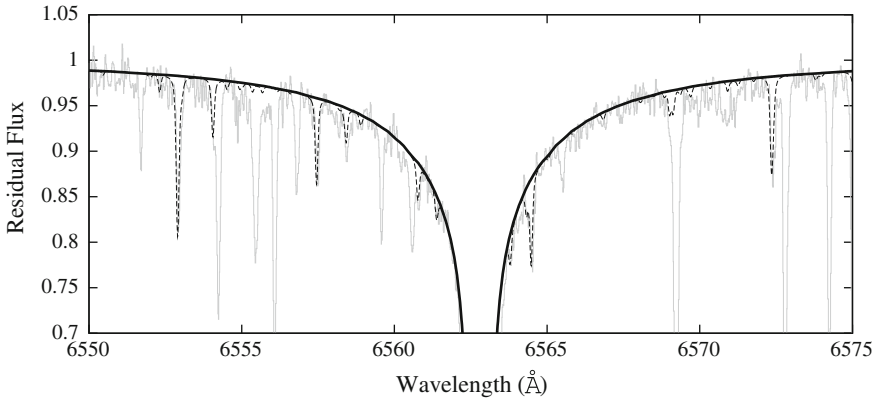

Fig. 4 The HERMES Hα profile of KIC 11772920 (*grey line*). The *black line* is the fit to the spectrum with $T_{\rm eff}$ = 5,300 K. Note that in addition to the presence of stellar absorption lines, there are several telluric lines arising due to water vapour in the Earth's atmosphere (*dashed-line*)

a $T_{\rm eff}$ of around 7,500 K. Note that rotation does not have a significant effect on the wings, only the core region, which as noted above we do not use in our fitting.

4 Spectral Line Depth Ratios

Spectral lines are sensitive to temperature variations within the line-forming regions. Line strength ratios can be used as temperature diagnostics, similar to their use in spectral classification. Gray and Johanson (1991) used line depth ratios to determine stellar effective temperatures with a precision of $\pm$10 K. While this method can

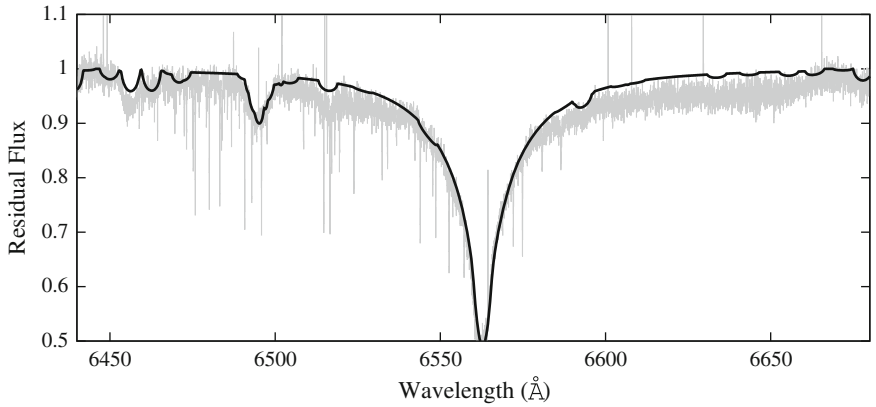

Fig. 5 The HERMES Hα profile of KIC 11090405 (*grey line*). The *black line* is the fit to the spectrum with $T_{\rm eff}$ = 7,500 K. Note the presence of sharp telluric absorption lines in the spectrum of this rapidly rotating star ($v \sin i = 120\,{\rm km\,s^{-1}}$).

yield very precise relative temperatures, the absolute calibration onto the $T_{\rm eff}$ scale is much less well determined (Gray 1994). This method is ideal for investigating stellar temperature variations (Gray and Livingston 1997).

5 Equivalent Width

The equivalent width (W_λ or just EW) is a widely-used measure of the strength of a spectral line:

$$W_\lambda = \int_0^\infty (1 - R_\lambda)\, d\lambda,$$

where R_λ is the residual flux at the given wavelength (λ). It is used in the determination of both stellar parameters and elemental abundances. It does, however, contain no information on shape of the line profile. While the truncation of strong wings can affect the measurement, as can uncertainties in the location of the continuum, it is line blending that is the most dominant source of uncertainties in EW measurements.

6 Metal Line Diagnostics

In a detailed spectral analysis, the equivalent widths of many lines are often measured. These can be used to determine the atmospheric parameters via metal line diagnostics:

- **Excitation Potential**
  Abundances from the same element must agree for all excitation potentials.

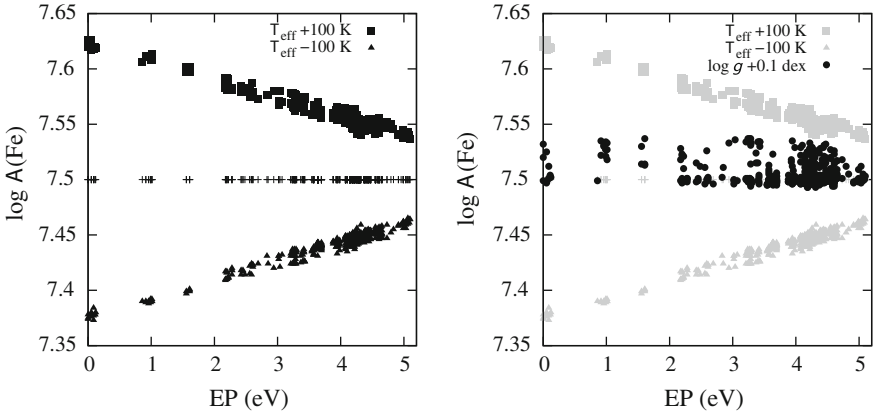

Fig. 6 The effect of changing $T_{\rm eff}$ (*left*) and changing $\log g$ (*right*) on the correlation between $\log A$(Fe) and EP

- **Ionisation Balance**
  The abundances obtained from differing ionisation stages of the same element must agree. The Fe I/Fe II ratio can be used as a $T_{\rm eff}$—$\log g$ diagnostic.

6.1 Exploring the Excitation Potential

When using the lower-level excitation potential (χ or just EP) to determine $T_{\rm eff}$ it is best to use lines that are not pressure sensitive. In the case of Solar-type stars use neutral metals, while in hotter stars use ionised metals. In both cases weak lines should be used to avoid the effects of saturation.

In order to investigate the use of excitation potential as a temperature diagnostic, a set of simulated 'observed' equivalent widths (W_0/λ) were generated using an ATLAS9 model with $T_{\rm eff}$ = 6,000 K, $\log g$ = 4.5 and $\log A$(Fe) = 7.50. The Fe I lines were taken from the Kurucz `gfall` line list in the wavelength range 5,000–6,000 Å. Only lines with calculated equivalent widths in the range 5–100 mÅ were retained.

Figure 6 shows that the change in slope caused by changing $T_{\rm eff}$ is clearly evident. However, variations in $\log g$ do not introduce a significant slope, but do increase the scatter in abundance. Of course, when using real data the observational uncertainties and errors in atomic data will introduce scatter into the trends.

The analysis method searches for null correlation between $\log A$(Fe) and EP (Santos et al. 2000). This can be by a linear regression fit and finding where the gradient is zero, or by finding where the linear-correlation coefficient is zero. Either method should yield the same result.

The uncertainty on $T_{\rm eff}$ can be taken to be the 1-σ error on gradient or correlation coefficient (Neuforge-Verheecke and Magain 1997). Another source of error is

uncertainties in equivalent widths, where in our example a 1% error in W_λ gives $\sim$10 K in $T_{\rm eff}$, 5 % 50 K and 10 % 100 K. In addition, there is a small but non-negligible influence by surface gravity, $\pm$0.1 dex in $\log g$ gives $\pm$20 K in $T_{\rm eff}$.

6.2 Equivalent Width Correlation

It could be argued that from a 'philosophical' viewpoint all the Fe I lines in an homogeneous stellar atmosphere must have the same abundance. Thus, we ought to use the differences in predicted line strengths as a diagnostic. Given that $\log\left(\frac{W_\lambda}{\lambda}\right) \propto \log A$ we can change the above procedure to use equivalent width differences. Let us use:

$$\log\left(\frac{W}{\lambda}\right) - \log\left(\frac{W_0}{\lambda}\right) = \log\left(\frac{W}{W_0}\right),$$

where W_0 is the observed equivalent width and W_λ is the calculated value for a given abundance.

The $T_{\rm eff}$ diagnostic is very similar, i.e. finding the lack of correlation between $\log\left(\frac{W_\lambda}{\lambda}\right)$ and EP. However, now we have to assume an abundance, which in our example is $\log A({\rm Fe}) = 7.50$.

The effects of changing $T_{\rm eff}$ and $\log g$ are very similar to previously, but with more scatter when varying $T_{\rm eff}$ and noticeably less scatter when varying $\log g$ (Fig. 7 top panels). However, since we have to assume an initial abundance, this value may not be correct. The lower-left panel of Fig. 7 shows the effect of changing $\log A({\rm Fe})$ by $\pm$0.1 dex; the overall trend is broadly horizontal, but the scatter is significantly enhanced. The scatter can be reduced by varying both $T_{\rm eff}$ and $\log A({\rm Fe})$ (Fig. 7 lower-right panel). In these cases, there is still a trend with EP, indicating that the parameters are not correct, but adding some noise and selecting less lines might give an acceptable result. Hence, using EW differences rather than calculating individual line abundances, appears to produce a slightly less acceptable procedure.

6.3 "Total" Equivalent Width

In order to abstract the method further, rather than using individual equivalent width differences, one could use the sum of the differences:

$$\sum \log\left(\frac{W}{W_0}\right).$$

In this case, rather than trend with EP, there is just one number per given $T_{\rm eff}$, $\log g$ and $\log A({\rm Fe})$ combination. The solution is now one of the combinations where the

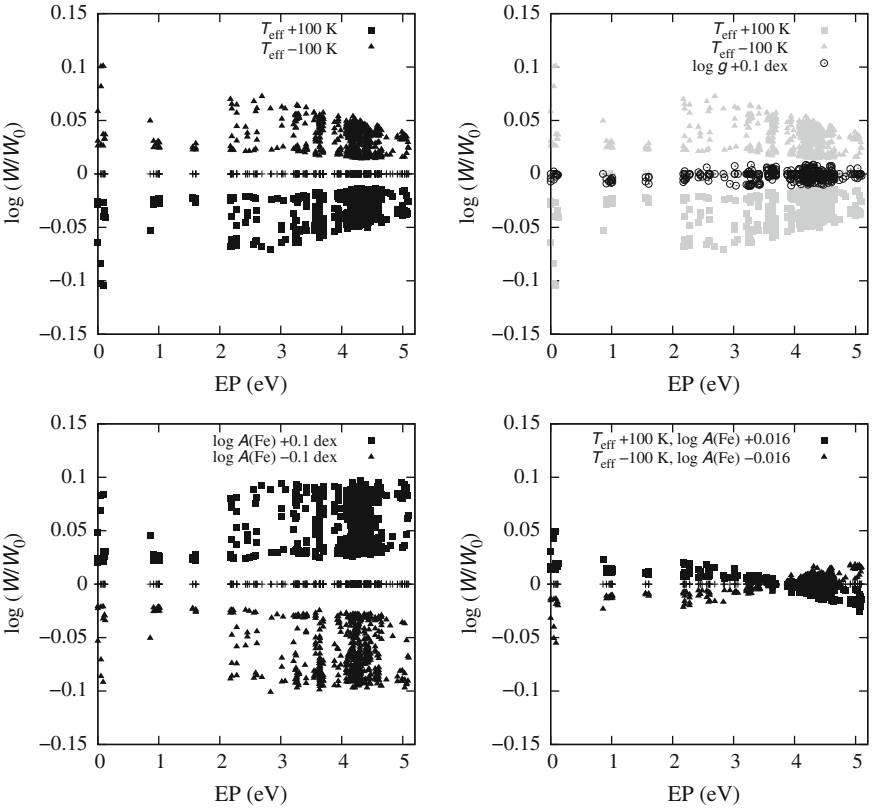

Fig. 7 The effects on the correlation between EP and $\log\left(\frac{W_\lambda}{\lambda}\right)$ of changing $T_{\rm eff}$ (*top left*), $\log g$ (*top right*), $\log A$(Fe) (*bottom left*), and both $T_{\rm eff}$ and $\log A$(Fe) (*bottom right*)

sum is zero, but which one? Thus, it would appear that using this method would result in a loss of information. However, Fig. 8 shows that while there is a trend with $\log A$(Fe), $T_{\rm eff}$ is virtually insensitive to $\log g$. Hence, provided a good value (or estimate) of $\log A$(Fe) is available, a sensible value of $T_{\rm eff}$ can be obtained.

6.4 Using χ^2

Measuring equivalent widths might not always be practical. For example, where there is severe line-blending, high rotation, etc. In these cases, we have to use spectrum synthesis methods in order to fit the spectrum to determine $T_{\rm eff}$.

Now consider $T_{\rm eff}$ determination using χ^2-fitting to spectrum. Using the same model as before, a synthetic 'observational' spectrum was generated using *all* spectral lines stronger than 5 mÅ in the wavelength range from 5,000 to 6,000 Å. In the χ^2

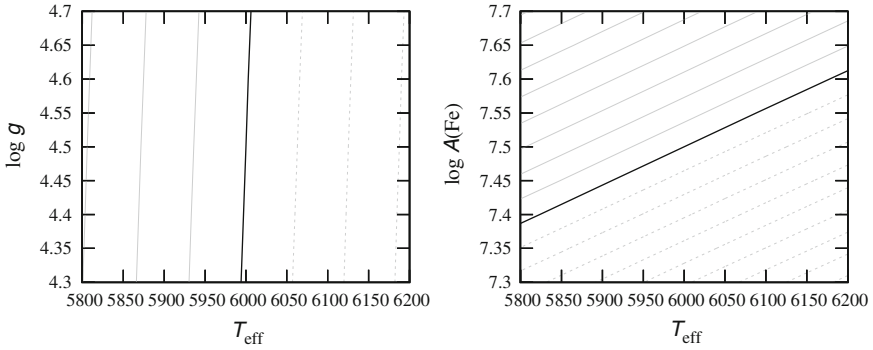

Fig. 8 The variation of "total" EW, $\sum \log(\frac{W}{W_0})$, for $\log g$ against $T_{\rm eff}$ (*left*) and $\log A$(Fe) against $T_{\rm eff}$ (*right*). While there is virtually no dependence on $\log g$, there is a strong correlation of $T_{\rm eff}$ with $\log A$(Fe)

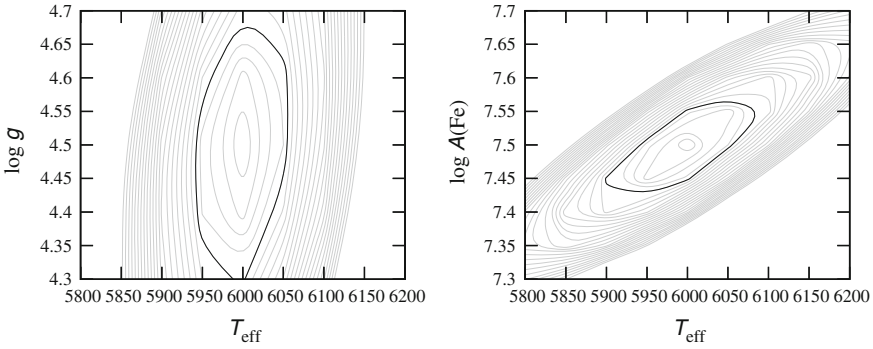

Fig. 9 χ^2 correlations, for $\log g$ against $T_{\rm eff}$ (*left*) and $\log A$(Fe) against $T_{\rm eff}$ (*right*). While there is virtually no dependence on $\log g$, there is a strong correlation of $T_{\rm eff}$ with $\log A$(Fe). The *darker line* gives the 1-σ error ellipse

calculation a signal-to-noise ratio of 100:1 was assumed, but no noise was added to the synthetic spectra.

As can be seen in Fig. 9, rather than a line in the diagrams, there is now a region of uncertainty—an error ellipse. As previously, there is a correlation between $\log A$(Fe) and $T_{\rm eff}$, but only a weak sensitivity to $\log g$. Further details on χ^2-fitting methods are given in Sect. 7.

6.5 Conclusions on Simulations

Using $\log A$(Fe) versus EP provides for a good determination of $T_{\rm eff}$, with low sensitivity to $\log g$. However, the other methods (EW, 'Total' EW, and χ^2) all have a $\log A$(Fe) complication, owing to the correlation between $T_{\rm eff}$ and $\log A$(Fe) and the

need to adopt or assume a value for log A(Fe). Nevertheless, using χ^2 gives regions of best fit, even though $T_{\rm eff}$ might be coupled with log A(Fe), but not (significantly) with log g. Adding noise and uncertainties in atomic data and model physics, will further complicate the analysis and, potentially, add unwanted systematics into the results.

7 Global Spectral Fitting

As mentioned in Sect. 6.4, an alternative to a detailed analysis of individual spectral line measurements, is to use the whole, or part, of the observed stellar spectrum and find the best-fitting synthetic spectrum. This is done by varying various input parameters, such as $T_{\rm eff}$, log g, metallicity ([M/H]), microturbulence ($\xi_{\rm t}$), and projected rotational velocity ($v \sin i$), etc., in order to find the combination that has the lowest χ^2 value. There are two commonly used procedures. The first is to take initial starting values for the input parameters and use a χ^2 minimization algorithm, such as Nelder-Mead downhill simplex or Levenberg-Marquardt, to find the best-fitting solution (e.g. Valenti and Piskunov 1996). The second is to take a large multi-dimensional grid of precomputed synthetic spectra for the various combinations of input parameters and search the whole grid to find the best-fitting solution (e.g. Lehmann et al. 2011).

The benefit of these methods is that they can be automated for vast quantities of stellar observations and can be used for spectra that are severely blended due to low resolution or rapid rotation (Hill 1995; Tkachenko et al. 2013).

Naturally, the final parameters are model-dependent and only as good as the quality of the model atmospheres used. The internal fitting errors only gives a measure of the precision of the result and is thus a lower-limit uncertainty on the parameters. Determination of the accuracy of the parameters requires the assessment of the results, using the exact same methods, to spectra of fundamental stars.

8 Do We Care About $T_{\rm eff}$?

It may appear strange, but the effective temperature of a star is not important; it is the T(τ_0) relationship that determines the spectral characteristics (Gray 2008). Hence, the parameters obtained from spectroscopic methods alone may not be consistent with the true values as obtained by model-independent methods. This is not necessarily important for abundance analyses of stars, but it is an issue when using the parameters to compare with fundamental values or to infer the physical properties of stars.

9 Conclusion

The effective temperature for a star can be obtained by several different techniques. By using a combination of these we can assess the quality of our parameter determinations. While some techniques can give precise $T_{\rm eff}$ values to ± 10 K, the overall accuracy of the values is significantly less and sometimes difficult to evaluate. At present $T_{\rm eff}$ determinations are generally accurate to no better than 1–2 % (50–100 K). Hence, always beware of $T_{\rm eff}$ values without error bars!

References

Appourchaux T, Chaplin WJ, García RA et al (2012) A&A 543:A54
Bruntt H, Bedding TR, Quirion P-O et al (2010) MNRAS 405:1907
Cayrel R, van't Veer-Menneret C, Allard NF, Stehlé C (2011) A&A 531:A83
Gray DF (2008) The observation and analysis of Stellar photospheres, 3rd edn. Cambridge University Press, Cambridge
Gray DF (1994) PASP 106:1248
Gray DF, Johanson HL (1991) PASP 103:439
Gray DF, Livingston WC (1997) ApJ 474:802
Heiter U, Kupka F, van't Veer-Menneret C et al (2002) A&A 392:619
Hill GM (1995) A&A 294:536
Lehmann H, Tkachenko A, Semaan T et al (2011) A&A 526:A124
Neuforge-Verheecke C, Magain P (1997) A&A 328:261
Raskin G, van Winckel H, Hensberge H et al (2011) A&A 526:A69
Santos NC, Israelian G, Mayor M (2000) A&A 363:228
Smith KC, van't Veer C (1998) Elemental abundance analyses. In: Adelman SJ, Lanz T (eds) Proceedings of the IAU working group on AP Stars Workshop, Institut d'Astronomie de l'Universite de Lausanne, p 133
Tkachenko A, Lehmann H, Smalley B, Uytterhoeven K (2013) MNRAS 431:3685
Uytterhoeven K, Moya A, Grigahcène A et al (2011) A&A 534:A125
Valenti JA, Piskunov N (1996) A&AS 118:595